East European Journal of Physics. 1. 191–202 (2026)
DOI: 10.26565/2312-4334-2026-1-19 ISSN 2312-4334

DFT STUDY OF THE STABILITY, ELECTRONIC, OPTICAL, AND THERMAL PROPERTIES OF TWO-DIMENSIONAL $BiBr_3$ SEMICONDUCTOR

Yadgar Hussein Shwan*, **Majida Ali Ameen**, **Aras Saeed Mahmood**
Physics Department, College of Education, University of Sulaimani, Sulaymaniyah 46001, Kurdistan Region, Iraq
*Corresponding Author e-mail: yadgar.shwan@univsul.edu.iq
Received September 24, 2025; revised February 14, 2026; accepted February 17, 2026

Density functional theory (DFT) serves as a first-principles method to thoroughly investigate the stability of the structure and analyse the electronic, optical, and thermal characteristics of two-dimensional bismuth tribromide (2D $BiBr_3$). Ab-initio molecular dynamic (AIMD) simulations reveal that the structure is thermally stable at 300 K. The $BiBr_3$ behaves as a semiconductor with a 2.84 eV band gap according to its electronic band structure and partial density of state (PDOS) analysis. Optical characterisation reveals that $BiBr_3$ has strong interactions in visible and ultraviolet wavelength domains, which shows its potential in the next-generation of optical and optoelectronic devices. A remarkable Seebeck value estimated via Boltzmann transport calculations, highlights the promise of $BiBr_3$ in low-temperature thermoelectric management. This investigation implies temperature-driven power factor improvement, peaking at 3.25×10^{12} W/K^2·cm·s at 300K. The $BiBr_3$ exhibits moderate heat capacity at intermediate to high temperatures while keeping very low thermal conductivity. This highlights its ability to effectively manage heat and serve as an insulator in various applications. The detailed results show that 2D $BiBr_3$ is a potentially favorable material with diverse possibilities in most technological applications.

Keywords: *$BiBr_3$ structure; DFT; Stability; Electronic characteristics; Thermal properties; Optical characteristics*

PACS: 71.15.Mb, 71.20.-b, 78.20.-e, 72.20.Pa, 65.40.-b

1. INTRODUCTION

Andre Geim and Konstantin Novoselov made an extraordinary discovery of graphene through their conventional mechanical exfoliation process known as the "Scotch tape method" in 2004. This discovery started the exploration of two-dimensional (2D) materials. A breakthrough in materials research is sparked by graphene, just one sheet of atoms of carbon organized in a hexagonal lattice, which demonstrated remarkable hardness, thermal characteristics, and electrical conductivity. After discovering graphene, scientists look for more 2D substances with special features. Molybdenum disulfide (MoS_2) is one example of a transitional metals dichalcogenide (TMD), a family of semiconducting materials having adjustable optical and electronic characteristics. Additional types of 2D materials follow these [1, 2].

In the past few years, the interest in 2D compounds is increasing because of their distinctive characteristics and prospective uses. Black phosphorus, Hexagonal Nitride of Boron (h-BN), and other metallic halides are among the 2D materials, their outstanding electronic characteristics and their use in future technology have made them an intriguing group of materials. The lower dimension of 2D structures results in enhanced carriers mobility, adjustable band structures, and quantum-confined effects, which in turn cause the spacial electronic behavior. Following an analysis of the electronic band structures of the crystals by electronic band structure, estimated band gap, and DOS revealed that Mg_3BiBr_3 exhibits semiconductor behavior [3, 4, 5].

An instance of the halide family, bismuth tribromide $BiBr_3$ is developed into a centre of scrutiny over the last decades. Achieving plenty of recognition due to its exceptional properties than its potential applications, setting up such a hybrid framework will enable the efficient calculation of a wide range of materials features, including thermal conductivity, electronic behavior, and optical properties, making it an appealing candidate for photovoltaics and light-emitting diodes, particularly in the fields of materials science and optoelectronics. Moreover, $BiBr_3$ shows potential for eco-friendly solutions in next generation energy devices as a lead-free substitute for conventional perovskites. Triple bromine Br atoms coordinated the bismuth Bi atom in $BiBr_3$ to produce a deformed octahedral shape in a (+3) oxidized state. Because the Bi^{+3} ion has just one pair of electrons, the deformation is caused by unequal bond lengths and angles, because it introduces hybridization effects that affect the position of the valence and conduction bands, this stereochemical activity has a substantial impact on the electronic characteristics [6, 7, 8].

$BiBr_3$ requires thermal stability to be employed in a variety of circumstances. According to DFT calculations, $BiBr_3$ has a sufficiently stable structure under ambient circumstances, which is important for device sustainability and stability in real-world situations as well as efficiency of the device. Theoretical research implies that BiI_3 in a crystalline-monolayer form would have less stability when compared to $BiBr_3$. $BiBr_3$ has been studied for its electronic characteristics, such as band structure and density of state, to better understand material characteristics. The indirect band gap of $BiBr_3$ is around 2.84 eV, positioning it in the visible to ultraviolet wavelengths. $BiBr_3$ has strong optical characteristics, such as UV-visible absorption of light and its high refractive index, they can lead to an enhancement of solar cell performance. Its optical

Cite as: Y.H. Shwan, M.A. Ameen, A.Sa. Mahmood, East Eur. J. Phys. 1, 191 (2026), https://doi.org/10.26565/2312-4334-2026-1-19

band gap and absorption coefficients make it a promising option for use in solar energy harvesting devices, $BiBr_3$ has a large dielectric constant, indicating the ability to storage electrical energy in an electrostatic field [9, 10, 11].

In terms of thermoelectric properties, DFT has emerged as a popular computational approach for studying 2D materials on an atomic scale, which gives information on numerous thermoelectric parameters such as the seebeck coeffcient, S, elecrical conductivity, σ, electronic thermal conductivity, κ, and the power factor, PF, of the system. They are chemical potential-dependent and temperature-dependent behaviors that indicate the components leading to their thermal resilience. In solar cell device, BiBr3 being a lead-free material has been investigated as a safer alternative[12, 13].

Limitations such as incomplete characterisation and insufficient examination of the properties have plagued studies of $BiBr_3$. This work attempts to fill these gaps by conducting a comprehensive and in-depth assessment of $BiBr_3$, which can provide a deeper understanding of its characteristics and its uses. This study uses DFT to analyse the stability, thermal, electronic, and optical characteristics of the $BiBr_3$ structure. DFT provides an excellent basis for studying the electronic structure of $BiBr_3$ at the atomic level, allowing precise predictions of its behaviour in many applications. We utilize AIMD to examine BiBr3's thermal stability and potential tolerance for heat by simulating its thermal properties. While optical feature computation suggests great potential for usage in a range of several areas, also, understanding the light-matter interaction is critical because it allows us to optimise materials for specific uses. Applying BoltzTraP to the Boltzmann transport framework, the thermoelectric performance at low temperatures and the heat capacity, phonon group velocity and lattice thermal conductivity at high temperatures are investigated [5, 14, 15, 16, 17].

2. METHODS AND COMPUTATIONAL TOOLS

We examine a two-dimensional unit cell of $BiBr_3$ with space group $P2_1/c$ consisting of 16 atoms. Quantum espresso utilizes the projector augmented wave (PAW) framework for conducting first-principles calculations. Furthermore, the GGA (generalized gradient approximation) is employed as a method to compute exchange and correlation terms when using PBE conceptual framework. A convergence test establishes the suitable kinetic energy cutoff for Brillouin zone sampling through testing. A combination of a $7\times7\times3$ Monkhorst-Pack k-point grid and a 45 Ry plane-wave cutoff is used as the computational parameters. The *nscf* calculations require a denser k-point grid of $50\times50\times5$ for their execution. Unit cell and atomic arrangements undergo structural relaxation through the relax and vc-relax modes to determine optimal structures suitable for detailed analysis. The relaxation energy reaches convergence at 4×10^{-7} eV [17, 18].

The AIMD simulation run tests thermal stability on a unit cell maintained at 300 K for 5 ps. Structure undergo analysis of their electronic and optical characteristics when they reach full relaxation, where stress are less than 6×10^{-4} eV/Å. The analysis of electronic transport characteristics employs BoltzTraP, which applies Boltzmann transport equations to constant relaxation time condition, important characteristics including the seebeck,S, electrical conductivity, thermal conductivity of electron, and power factor are calculated. Phonopy program calculates entropy and heat capacity by appling the small displacement approach [19]. The Phono3py software is used to calculate the conductivity of lattice vibration and group velocity, employing a q-point mesh of 10×10×7. XCRYSDEN and BURI 1.3. are used to visualize and design structures, as well as to improve our understanding of material characteristics by assuring correct modeling and guiding investigations [12, 20, 21].

3. RESULTS

This part discusses the results of the stability, electronic, optical, and thermal properties of the 2D $BiBr_3$ structure.

3.1. Geometric properties

The $BiBr_3$ crystallizes as a structure that is monoclinic in the $P2_1/c$ space group, arranged in a two-dimensional form. In this arrangement, every bismuth (Bi^+) ion is linked to by triple bromine (Br^-) ions, giving rise to edge-sharing $BiBr_3$ octahedra. Modeling simulations to determine the electronic, thermal, and optical characteristics of $BiBr_3$ needs accurate descriptions of geometric aspects, including unit cell, lattice constants, and lengths of bond. Geometric variation factors significantly influence the electronic band structure, phonon dispersion, and optical response, emphasizing the need for computational studies that include an accurate assessment of the atomic configuration [22, 23].

After fully relaxed structure, the lattice constants are $a = 7.40$Å, $b = 12.79$Å, the z vacuum distance is assumed to be $c = 7.69$ Å, and the Bi-Br bond length is found to be 2.90 Å. They are decsribing the arrangement of atoms in a unit cell. The Fig. 1(a),(b) depicts the top and side perspectives of the structure. The study analyzes the characteristics of $BiBr_3$ by utilizing a relaxation structure-optimized lattice parameter. The findings are consistent with reported data [24].

3.2. Stability

We evaluate formation energy to ensure that the structure becomes energetically stable. The formation energy of a $BiBr_3$ material refers to the overall energy required to develop it based on its separate components in their normal states. Negative formation energy means that the material energetically is great stable, whereas positive formation energy demonstrates the fact that the material is unstable and might degradation, the $BiBr_3$ becomes energiticaly excellent stable at lattice distance of 7.40 Å due to its minimum negative formation energy of -2.45 eV [25].

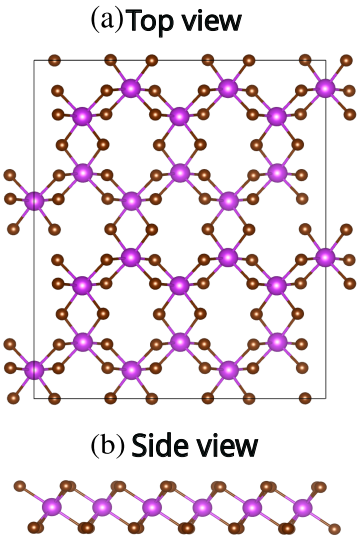

Figure 1. Structure of 2D $BiBr_3$ from top view (a), and side view (b).

To evaluate the thermal stability of $BiBr_3$, we are applied AIMD to compute temperature and total energy versus time (5 ps) in a unit cell at 300 K. The temperature variation increases somewhat at the start of the simulation due to the structure requires only a brief amount of time for reaching equilibrium. Then the fluctuation becomes roughly constant throughout time, indicating that the structure has achieved stability and it is in an equilibrium phase. Additionally, the temperature profile varies little during the simulation, indicating that heat transport is restricted by a $BiBr_3$ structure as seen in Fig. 2(a) . We are noticed no substantial structural disturbances or bond breaks, this corresponding to the system remain stable.

The energy fluctuations of roughly 0.22 Ry, which is inside the range reported in earlier. The $BiBr_3$ structure showed no substantial energetic changes throughout the simulation period, thus avoiding any structural deformation. It is apparent that there is no structural change in terms of energy as illustrates in Fig. 2(b). $BiBr_3$ may have an extremely rigid lattice structure or strong bonds due to its low (temperature and energy) fluctuations. These little fluctuations demonstrate that phase transitions or breakdowns do not take place with time. $BiBr_3$ is stable and crucial for structural integrity. AIMD simulations provide a useful foundation for testing structural stability [26, 27].

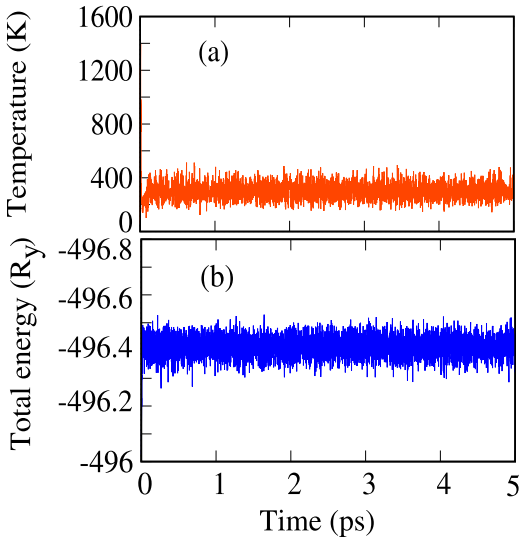

Figure 2. The flactuation of temperature (a), and energy (b) versus time during the AIMD simulation.

3.3. Electronic properties

We first calculated $BiBr_3$'s thermal stability through analysis, then, the electronic properties of $BiBr_3$ are computed. It mostly depends on band structure and partial DOS, which are computed along the path $\Gamma \rightarrow Y \rightarrow M \rightarrow K \rightarrow H \rightarrow X$. Both are referenced to the same energy level where Fermi energy is taken to be zero, these are shown in Fig. 3 and Fig. 4.

The $BiBr_3$ material exhibits indirect bandgap characteristics because its electronic states are unevenly distributed across the band structure. The valence band's maximum (VBM) is located at the X point and the conduction band minimum (CBM) at the Y point, giving an indirect band gap. In these situations, the transition between the VBM and CBM requires a change in energy as well as momentum. This condition decreases the propensity of direct photon-induced transitions, since phonons are required to achieve momentum conservation. As a consequence, the optoelectronic transition of the material is inherently dictated by the indirect nature of the gap. Fig. 3 shows that the GGA-PBE functional may potentially underestimate the calculated indirect band gap of 2.84 eV. This underestimation is due to the fact that standard DFT that is based on semi-local exchange-correlation functionals is incomplete when it comes to the discontinuity in the exchange-correlation potential and tends to delocalize the electron densities [28].

The obtained band structure of $BiBr_3$ is not flat, which points to the high dispersion, delocalized electronic states, and to the strong variations of energy levels with momentum. The degree of band dispersion is proportional to the effective mass of charged carrier, $m^* = \hbar^2 \left(\frac{\partial^2 E}{\partial k^2}\right)^{-1}$. In such a way, the dispersive character of the band structure of $BiBr_3$, implies quite delocalized electrons and holes, resulting in a higher efficiency of the charge transport. The electronic band structure is determined by the arrangement of the atoms, which is significant in establishing its characteristics. Lower symmetry in $BiBr_3$ causes energy bands to spread widely due to fewer degenerate energy levels and generates substantial band gap, from this perception, this arrangement is not fully symmetrical in a high-symmetry sense, because there are some imperfections. Its depends on the specific observation or crystal phase [29].

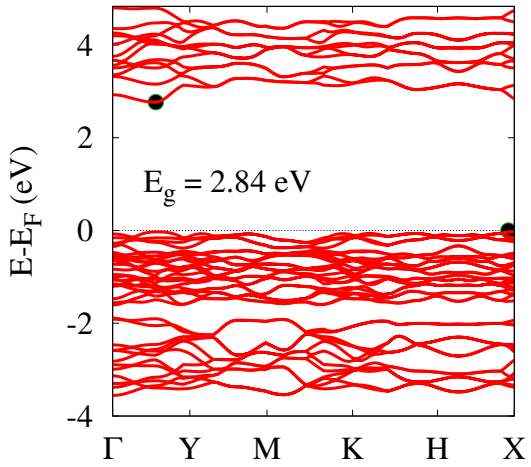

Figure 3. The electronic band structure of 2D $BiBr_3$, with the Fermi level referenced at zero energy.

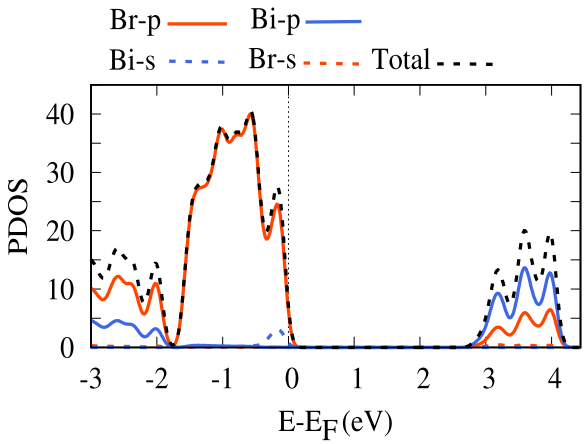

Figure 4. Project density of states (PDOS) and total density of state of 2D $BiBr_3$ material as obtained with DFT calculations.

A PDOS calculation is conducted for the constituent elements in the energy range of (-3 to 4.5) eV, highlighting their orbital contributions to the band structure, which is essential for a comprehensive understanding of bonding properties, as illustrated in Fig. 4. The predominance of Br-*p* orbitals in the valence band (VB) indicates a strong ionic character, stemming from the robust interaction between the bismuth and bromine atoms. Conversely, in the conduction band (CB),

Bi-p orbitals significantly influence both the electronic and optical characteristics of $BiBr_3$. The considerable electronic character separation between the Br and Bi atoms suggests the ionic nature of bonding in $BiBr_3$. Additionally, the band gap varies from 0 to 2.83 eV, indicating that the PDOS is zero due to the absence of allowed electronic states [30].

We are noticed that the two atomic orbitals involved in the reaction (Bi-p and Br-p) remained distinct due to the orbitals do not normally hybridize. The orbitals work independently without mixed and retain their original features, resulting in a localized disposition in states. The projected density of states (PDOS) calculations show a weak contribution from Bi-s and Br-s orbitals, as these states are at lower energies compared to the p orbitals, which limits their involvement in bonding. In heavy-element compounds, relativistic effects and the larger principal quantum number make s orbitals more contracted and lower in energy, further decreasing their overlap with nearby orbitals. As a result, these s orbitals play a minor role in the bonding framework. Conversely, the Bi-p and Br-p orbitals, which are higher in energy and more spatially extended, primarily drive the bonding interactions, forming the main electronic coupling in the system. In conclusion, $BiBr_3$ has an indirect band gap of about 2.84 eV that is smaller compared to that obtained in Bi_4O_6, reported as 3.12 eV [31].

3.4. Optical properties

This section analyzes optical characteristics (dielectric (ε), absorption coefficient (α), and optical conductivity of 2D $BiBr_3$ shape based on Random Phase Approximation (RPA) across the Brillouin zone with dense mesh grid points at span of energy (0-10)eV. These characteristics describe how a material responds to incoming electromagnetic spectrum. $BiBr_3$'s optical properties can be helpful for a variety of applications. The Fig. 5 shows how dielectric behavior changes with photon energy under both perpendicular (E_z) and parallel (E_x) electric field conditions [32].

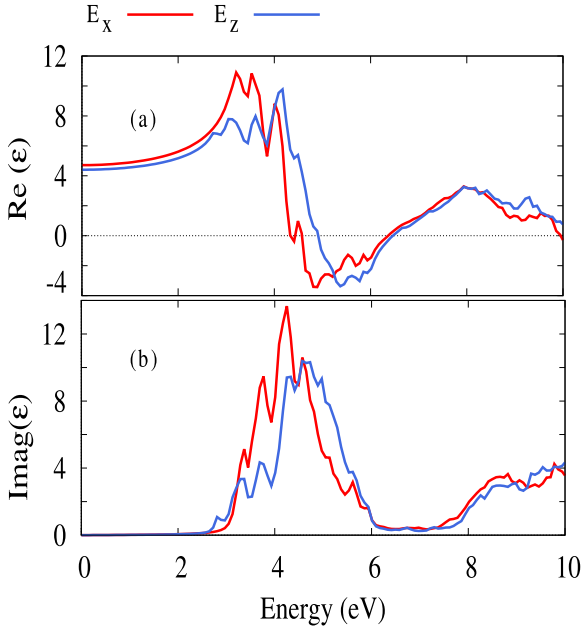

Figure 5. Real part, Re(ε), and Imaginary part, Imag(ε), of the dielectric function of 2D $BiBr_3$ in parallel, E_x (red) and perpendicular, E_z (blue) applied electric field.

It is noteworthy that the results in the x- and y-polarized electric field are comparable showing symmetric optical response of $BiBr_3$. However, the interactions varies in the electric field x-polarization and z-polarization, owing to weak anisotropic structure. The real part Re(ε) refers to the active aspect of structures that respond to electrical energy storage. The stationary dielectric function is 4.9 and 4.7 at zero photon energy for E_x, E_z respectively. This suggests that $BiBr_3$ exhibits strong polarization behavior or is easily polarizable, because of the their atoms are less sensitive to electric fields. The material displays its strongest response at around 3 eV. This occurs at particular photon energies where the electrons in the valence band can be polarized most efficiently by the incident electromagnetic field, typically around the point of interband transitions, the substance exhibits a robust electrical energy storage capacity when observed from this standpoint. At frequencies higher than this, the electrons are no longer able to respond in a meaningful way to the rapidly varying electromagnetic field, and Re(ε) will begin to drop. Around 4 eV, the material attains plasmonic behavior because the Re(ε) becomes negative due to the collective electron oscillation, making the material useful for plasmonic applications, at this point the material does not support propagating wave [33].

The imaginary part of dielectric reacte to a various frequncies, seen in Fig. 5(b). The Imag(ε) of the dielectric function corresponding to how much energy material absorbs. At low frequencies the static value of Imag(ε) is almost equal to zero since there is insufficient energy in the photons at low frequencies to excite electrons across the band gap.

As the energy of photons is successively increased and passes beyond the band gap threshold, Imag(ε) rises sharply because allowed electronic transitions between the valence band and the conduction band can then occur. Peaks at certain energies can be seen, each one being due to a strong optical transition at a critical point in the electronic band structure where the joint density of states is large. Their peaks represent the energy bands at which photon energy absorption is maximum. At higher photon energies Imag(ε) is gradually decreased due to lowering probability of additional elctronic excitations, and the electrons cannot react to the fast oscillations of the external field anymore. The Imag(ε) shares a connection with shielding capabilities through electromagnetic screening mechanisms present in materials. Shielding strength increases while Imag(ε) value increases and vice versa. Therefore the general tendency of Imag(ε) , which begins at nearly zero, increases with energy, reaches maxima associated with characteristic transitions, and decays at high frequencies, characterizes the primary absorption response of the substance [34].

Optical conductivity, descibes a material's capacity to transmit electric current under an oscillating an electric field. The optical conductivity varies significantly with respect to photon energy as it is illustrated in Fig. 6. The key point is, the optical conductivity in the range energy (0-2.82) eV dis effectively zero, because there aren't many electronic states accessible for optical transitions. Also, it is denoted as the optical band gap. The transition from the valence to the conduction band appears clearly with the maximum optical conductivity of $BiBr_3$ happening at 4.1 eV, the material shows strong light-absorbing properties and transition abilities that function at multiple photon frequencies. The photon energy surpassing the band gap plays a vital role in determining the total transition strength and involvement of most interband transitions. Multiple allowable transitions contribute to the observed peak. This information allows us to comprehend charge transfer patterns, which are required by developers for the production of storage device applications. Although photons with more energy can potentially cause promotion across larger energy gaps, the number of available and strongly coupled transitions is reduced. Optical coupling becomes weaker as the reduced joint density of states, which leads directly to a reduced optical conductivity at high energy photons [35].

The refractive index, n, of a substance is a dimensionless number that defines the way light travels through material as displays in Fig. 6, and its govens phase velocity and dispersion. $BiBr_3$ refractive index varies with wavelengths due to frequency-dependent refractive index. The static n is 2.24 at zero photon energy, indicating the material strongly respond to electric field. At low photon energies (below the band gap), no interband transitions happen, so Imag(ε)$\approx$ 0, and Re (ε) remains fairly constant. As a result, the refractive index stays nearly the same. Beyond this point the refractive index grows smoothly because the light phase velocity decreases and normal dispersion. Then at 4 eV, the refractive index gradually reduces because the energy of the photon is more than the band gap of the material, leading to the saturation absorption of the material, As photon energy rises, the oscillation becomes too rapid for bound electrons to react effectively. Then, the Polarisation weakens and declines, resulting in a reduction of n is occur [36].

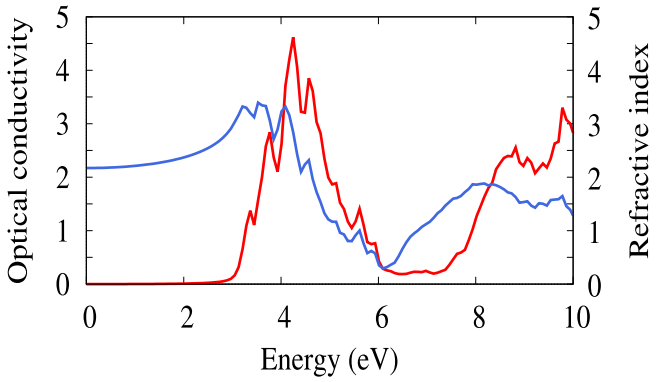

Figure 6. Optical conductivity (red), and refractive index (blue) of 2D $BiBr_3$ in external electric field.

The absorption coefficient α governs a material's ability to absorb photons at various of energy as illustrated Fig. 7. The α value starts at zero during the initial part of the curve since the photon energy lacks sufficient power to promote carriers from VB to CB. A steep rise in α occurs when photon energy matches the band gap energy, which is roughly 2.83 eV, corresponding to the Imag(ε) curve. Analysis indicates the structure demonstrates a distinct absorption peak at around 4.5 eV that belongs to the UV spectrum. The detection of VIS and UV light through this curve is essential for solar enegy applications. $BiBr_3$ has the capacity to absorb in the VIS to extreme-UV spectrum. At extremely high photon energies, the absorption coefficient decrease, mostly because the material no longer has accessible states for electronic transitions at that range of wavelength and he available electronic states become less responsive to photons carrying higher amounts of energy and result in decreased absorption capability [37].

The reflectivity of $BiBr_3$ is displayed in Fig. 7. From 0.0 eV to 2.74 eV, the reflectivity has a value of nearly 0.15%. At low photon energies (below the band gap), the free-electron dielectric response is weak. This means the material doesn't effectively reflect light, leading to very low reflectivity in that range. As photon energy increases above the band gap, reflectivity rises-potentially reaching values as high as 57% on average. This is because electrons can oscillate more strongly in response to the light. The reflectivity can be reduced to levels almost reaching zero at hight frequency. At

this photon energy, the incident light is extremely transparent through it, as reflection is suppressed and absorption is negligible. Provided that this happens at around 7 eV, the material would effectively look transparent in that very limited ultraviolet wavelength. From this analysis, this material can be used as shielding in the UV range.

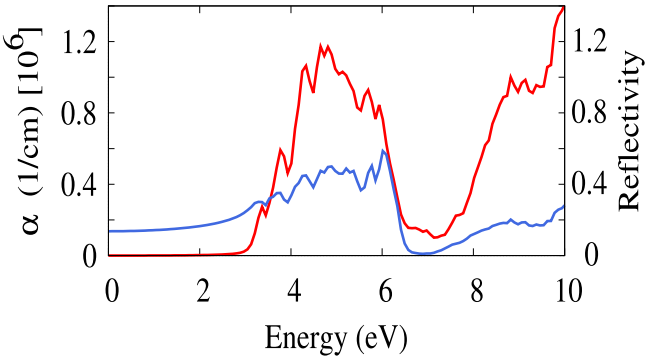

Figure 7. The absorption coefficient,α, (red) and reflectivity (blue) of $BiBr_3$ as a function of the energy of the photon in the presence of external electric field.

3.5. Thermal properties

The thermal properties will be analyzed through two unique temperature ranges known as low temperature and intermediate of high temperature. The analysis of electronic thermal response in materials under low-temperature conditions serves to determine fundamental thermoelectric parameters consisting of S, σ, κ, and PF as a function of chemical potential with energy of Fermi set to zero. $BiBr_3$ supports exceptional thermoelectric stability through Seebeck coefficient calculation across the studied temperature conditions, as shown in Fig. 8(a). The directional aspect of the Seebeck coefficient constitutes a crucial property for understanding material behavior. The sign of S reveals which charge carriers predominate in a material since positive S values indicate holes whereas negative S values indicate electrons. A thermal gradient operating near the E_F with $S > 0$ indicates holes act as dominant charge carriers through which heat transfer occurs by hot holes diffusing toward the cold region. Electron transport between the hot and cold sides results in negative S, indicating the presence of CB [38].

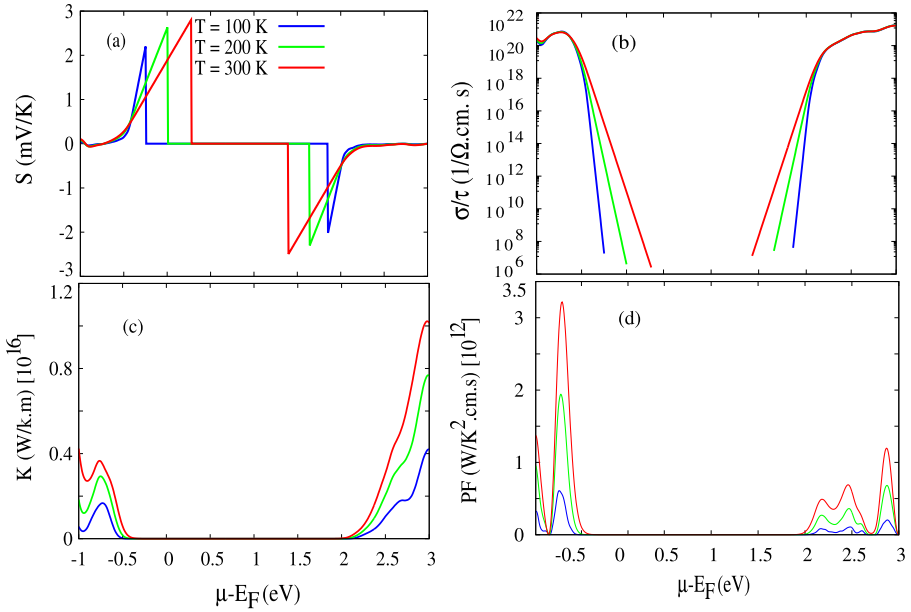

Figure 8. The Seebeck coefficient (a), electrical conductivity,the y-axis is scaled in a logarithms form (b),electronic thermal conductivity κ (c), power factor (d) of $BiBr_3$ versus μ-E_F for the different values of temperature. μ refers to the chemical potential.

The S value shows minimal change when the temperature rises from 100 to 200 K to 300 K since carrier density changes little due to gradients density of states (GDS) and weak scattering. Under a range of chemical potentials from -0.27 to 1.88 eV the S exhibits a plateaus region at 100 K where S equals zero because of unavailable band structure.

Rising temperature causes plateaus to become smaller because carrier excitation becomes more straightforward, resulting in increased sample smearing. The significant S value of $BiBr_3$ shows that it acts as a semiconductor material, and also raises PF while aligning with its application potential for energy conversion [39].

The electrical conductivity, σ, which is shown in Fig. 8(b) is plotted on a log scale because this will help to visualize better and discover a trend where it would be difficult to achieve with a realistic scale. The σ represents the flow of charge carriers within a material. The σ shows a strong correlation with chemical potential and temperature because these factors affect carrier concentration and distribution. The Values of σ that surround the VBM and CBM match the DOS peaks observed in the VB and CB. The σ occurs more efficiently in the CB compared to the VB because of differences in charge carrier behavior and DOS. There exists no density of the state between CB and VB resulting in zero electrical conductivity (null electrical). This state of affairs seems to favor the Seebeck effect. Electricity conductivity responds to temperature variations that modify the number of active charge carriers in the material. When the temperature surpasses zero the number of thermally excited electrons rises leading to increased smearing around the Fermi level that enhances the value of σ, which are roughly 10^{21} and 10^{22} 1/Ω.cm.s for VB and CB respectively. An increase in σ value tends to increase power factor, which corresponds to photovoltaic increase efficiency, especially hybrid solar cell device.

The electronic thermal conductivity,κ, which resembles the power factor pattern, is depicted in Fig. 8(c) in various low temperatures. The κ of $BiBr_3$ through electrons depends on multiple variables like σ behavior, carrier mobility and temperature variations. The thermal transport behavior of this material heavily depends on electron-mediated thermal conductivity. The value of κ increases as temperature rises due to thermal excitation of electrons that creates additional electron involvement in thermal transportation. The percentage values of κ increase by 114% and 150% for VB and CB, respectively, in the temperature range from 100 to 300 K based on Wiedemann–Franz law [40, 41]. The achievement of full κ may have been prevented by the occurrence of electron-electron collisions. Electron mobility changes because of scattering, which affects the value of κ, this interactions result in lower thermal conductivity levels . From this perspective, the excellent thermal conductivity of $BiBr_3$ enhances heat dissipation, which preserves the temperature of solar cells while increasing photovoltaic system efficiency and a long life [42, 43].

From the Fig. 8(d), the power factor of $BiBr_3$ depends on both chemical potential and temperature parameters for evaluating the material's charge carrier transport properties. A temperature increase shifts the chemical potential toward band edge positions, so it changes carrier densities and affects transportation properties. Low power factor values occur at low temperatures since carrier activation remains restricted. Still, as temperature increases leads to improved carrier excitation, which boosts σ and enhances S and that makes PF is high, the power factor shows its maximum value at the band edges VBM or CBM because these areas maintain an ideal balance between Seebeck coefficient and electrical conductivity and optimal carrier concentration. $BiBr_3$ demonstrates a better hole transport efficiency through the fact that its valence band maintains higher power factor values than its conduction band. The high PF value serves excellently for thermoelectric applications and it can be used as a hole transport layer in solar device energy [18].

After verifying thermal stability. At intermediate high temperature ranges, we analyze $BiBr_3$'s thermal properties through temperature-dependent measurements of heat capacity C_V and entropy, which appear in Fig. 9.

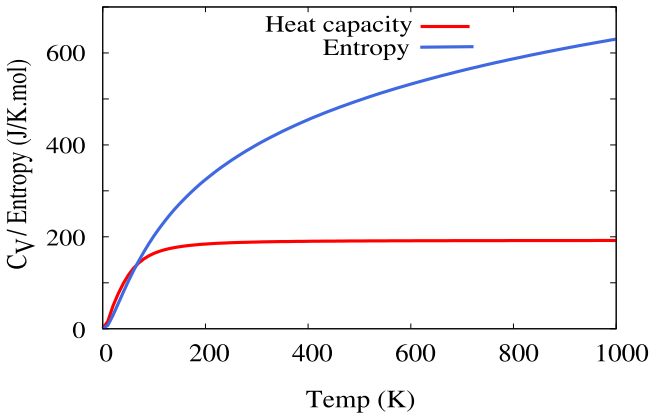

Figure 9. Heat capacity (red) and entropy (blue) as a function of temperature of $BiBr_3$.

$BiBr_3$'s heat capacity increases with temperature because of the continual activation of phonon modes, which is consistent with Debye's T^3 law (T < 300 K), where only low energy phonons contribute to heat capacity. Above 200 K, many of the phonon modes in the low- and mid-frequency spectrum are already excited. Only high-frequency modes are left to participate. Because these high-frequency modes must be excited with much greater energy, the heat capacity of the system grows more slowly with temperature. Consequently, the specific heat becomes nearly constant at high temperatures, this is referred to as the plateau region. The C_V of $BiBr_3$ exhibits moderate heat capacity, making it a potential candidate for energy storage, which is (12.35 J/K.mol at 300 K per atom). Despite this trend, the heat capacity of $BiBr_3$ does not attain the classical Dulong-Petit limit, even at elevated temperatures of 1000 K. This phenomenon can be attributed to an inadequate phonon population that fails to saturate C_V to the classical limit. Additionally, it is possible that the vibrational

modes in $BiBr_3$ do not fully contribute to the heat capacity at high temperatures, a factor that may be influenced by the presence of the heavy Bi atom [44, 45].

When temperatures reach a moderately high level the system entropy achieves an approximate value of 620 J/K·mol, which demonstrates notable lattice disorder. The material performance under extreme conditions would be affected by the elevated disorder since it impacts both structural quality and thermal characteristics. Complete randomness throughout the crystal lattice corresponds to high entropy values. An increase in temperature triggers the combined effects of intensified atomic vibrations and lattice defects and anharmonic interactions which create a disordered state in the lattice.

Lattice thermal conductivity is a measure of the efficiency of the heat conduction through a substance owing to lattice vibration, specifically phonons. Phonons are the main carriers of thermal energy in semiconductors and insulators, as shown in Fig. 10(a) [46]. The lattice thermal conductivity of $BiBr_3$ is temperature dependent. At a temperature of 200K, the lattice usually reaches a maximum of 4.4 W/m.K, this is because the phonon population rises due to normal phonon scattering (N-process) and does not disrupt heat flow much, as well as because of the high group velocity. At higher temperatures, many of the high-frequency phonons transport the majority of the thermal energy and become active, and the Umklapp scattering (U-process) dominates, phonons interact strongly and lose momentum, which reduces their capacity in conducting heat. As a result, conductivity of heat is reduced [47]. Studies indicate that phonons significantly affect the transfer of heat in various 2D monolayers, as demonstrated by research on other 2D materials [48, 49]. The $BiBr_3$ exhibits weak lattice thermal conductivity, which is attributed to the material properties that limit the phonon transport. Due to the presence of the heavy Bi element, atom vibrations occur at very slow rates, ensuring that group phonon velocities are reduced. This leads to reduced efficiency in the transport of heat. In short, $BiBr_3$ has a moderate heat capacity as well as low lattice thermal conductivity, rendering it a good thermal insulator.

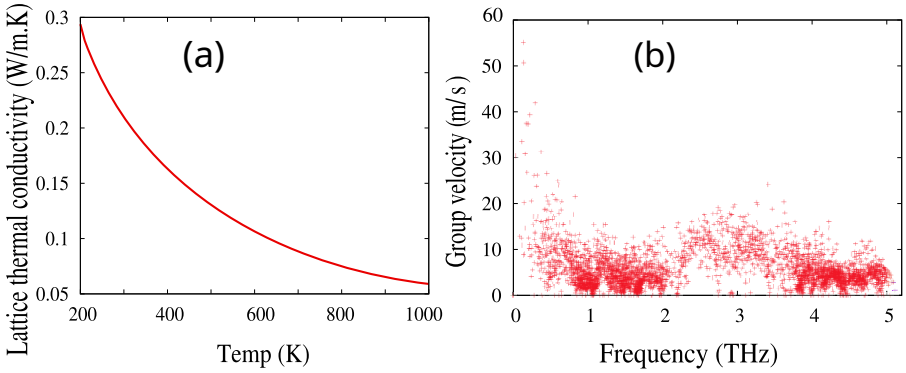

Figure 10. Lattice thermal conductivity (a), and group velocity (b) of $BiBr_3$.

Thermal transport is governed by the group velocity because the lattice thermal conductivity is proportional to the product of the phonon group velocity and the heat capacity. When the temperature rises, the lattice becomes softer, and as a result, the group velocity of phonons reduces, leading to lower lattice thermal conductivity, the trend of this behavior is reflected well based on the trends observed in $BiBr_3$ material, as can be seen in Fig. 10(a) and Fig. 10(b) [50, 51]. Phonon group velocities are large in the low-frequency regime (acoustic), indicating a fast propagation of the respective vibrational modes inside the $BiBr_3$ structure, which corresponds well to the speed of sound in the material. Conversely, at frequencies between (1-2) THz, the phonon group velocity remains mostly constant. This indicates that vibrational speeds stay relatively steady or increase gradually in this high-frequency range, the atoms participate in highly localized 'rattling' motions. The energy remains trapped there temporarily, which reduces thermal conductivity. Overall, the thermal properties of $BiBr_3$ make it an interesting candidate in many thermal management applications, especially when heat absorption and insulation play the most crucial role.

4. CONCLUSIONS

This study offers a comprehensive first-principles investigation of $BiBr_3$, uncovering its diverse properties through the DFT framework. The material exhibits exceptional thermal stability, maintaining structural integrity at high temperatures with minimal energy fluctuations. The $BiBr_3$ material acts as a semiconductor with an indirect band gap of 2.84 eV. Simultaneously, its optical interactions in the Vis-UV regions shows strong light absorption, making it a promising candidate for energy harvesting and lead-free photovoltaic applications. However, it is highly reflected in the UV range, which is roughly (59%). The large peak in the power factor and Seebeck indicates maximum transport efficiency at room temperature, reflecting an optimal balance between electrical and thermal properties suitable for energy conversion and thermal management. Its moderate heat capacity, remaining below the Dulong–Petit limit, combined with low lattice thermal conductivity, further supports its potential as an insulating material. $BiBr_3$'s unique electronic, optical, and thermoelectric properties position it as an ideal material for next-generation optoelectronics, energy harvesting, and thermal management applications.

Acknowledgment

This work was financially supported by the University of Sulaimani. The computations were performed on resources provided by the Computational Science Lab at Research and Developed Center at the University of Sulaimani. YHS has special thanks to Nzar Rauf Abdullah for fruitful discussions. This project is done as a part of PhD thesis.

ORCID

Yadgar Hussein Shwan, https://orcid.org/0000-0002-0020-253x; **Majida Ali Ameen**, https://orcid.org/0009-0004-9641-5186; **Aras Saeed Mahmood**, https://orcid.org/0000-0003-3908-3766

REFERENCES

[1] S.S. Prasad, R.K. Mishra, S. Gupta, S. Prasad, and S. Singh, "Introduction, History, and Origin of Two Dimensional (2D) Materials," in: *Advanced Applications of 2D Nanostructures. Materials Horizons: From Nature to Nanomaterials*, edited by S. Singh, K. Verma, and C. Prakash, (Springer, Singapore, 2021), pp. 1-9. https://doi.org/10.1007/978-981-16-3322-5_1

[2] X. Duan, and H. Zhang, "Introduction: two-dimensional layered transition metal dichalcogenides," Chem. Rev. **124**(19), 10619–10622 (2024). https://doi.org/10.1021/acs.chemrev.4c00586

[3] M. U. Khandaker, H. Osman, S. A. Issa, M. Uddin, M. H. Ullah, H. Wahbi, and M. Hanfi, "Newly predicted halide perovskites Mg_3-AB3 (A= N, Bi; B= F, Br, I) for next-generation photovoltaic applications: a first-principles study," RSC advances, **15**(8), 5766-5780 (2025). https://doi.org/10.1039/D4RA09093D

[4] K. S. Novoselov, A. K. Geim, S. V. Morozov, D.E. Jiang, Y. Zhang, S. V. Dubonos, I. V. Grigorieva, and A. A. Firsov, "Electric field effect in atomically thin carbon films," Science, **306**(5696), 666-669 (2004). https://doi.org/10.1126/science.1102896

[5] S. Abdu, A. Shu'aibu, M. Aboh, and M. Abubakar, "Computations of the band structure and linear optical properties of methylammonium bismuth bromide and methylammonium galluim bromide using FHI-aims code," Science World Journal, **14**(2), 101-105 (2019). https://scienceworldjournal.org/article/view/19450/13175

[6] S. Yosim, L. Ransom, R. Sallach, and L. Topol, "The bismuth-bismuth tribromide and bismuth-bismuth triiodide systems," The Journal of Physical Chemistry, 66(1), 28-31 (1962). https://doi.org/10.1021/j100807a006

[7] K. R. Kurbanov, and N. N. Kurbanova, "Structrural peculiarities and some electrical-and-physical properties of bismuth oxide and antimony trichloride and tribromide," Ph.D. thesis, Sumy State University Publishing House (2011).

[8] G. Huang, Y. Q. Sun, Z. Xu, M. Zeller, and A. D. Hunter, "Structural regularity and diversity in hybrids of aromatic thioethers and $BiBr_3$: from discrete complexes to layers and 3D nets, Dalton Transactions, (26), 5083-5093 (2009). https://doi.org/10.1039/B902490P

[9] Y. Xu, M. Lyu, and J. Zhu, "Surface engineering in CsPbX 3 quantum dots: from materials to solar cells," Materials Chemistry Frontiers, **8**(9), 2029-2055 (2024). https://doi.org/10.1039/D3QM00911D

[10] M. M. R. Al-Fartoos, A. Roy, T. K. Mallick, and A. A. Tahir, "Advancing thermoelectric materials: a comprehensive review exploring the significance of one-dimensional nano structuring," Nanomaterials, **13**(13) 2011 (2023). https://doi.org/10.3390/nano13132011

[11] X. Liu, Z. Wang, G. Yu, Z. Sun, G. Zhang, X. Q. Wang, L. Zhu, *et al.*, "Growth morphology of {1 0 1} surfaces of l-arginine trifluoroacetate crystals investigated by afm," Journal of Physics and Chemistry of Solids, **68**(4), 608-610 (2007). https://doi.org/10.1016/j.jpcs.2007.02.002

[12] P. Giannozzi, S. Baroni, N. Bonini, M. Calandra, R. Car, C. Cavazzoni, D. Ceresoli, *et al.*, "Quantum espresso: a modular and open-source software project for quantumsimulations of materials," Journal of physics: Condensed matter, **21**(39), 395502 (2009). https://doi.org/10.1088/0953-8984/21/39/395502

[13] S. Baroni, S. De Gironcoli, A. Dal Corso, and P. Giannozzi, "Phonons and related crystal properties from density-functional perturbation theory," Reviews of modern Physics, **73**(2), 515 (2001). https://doi.org/10.1103/RevModPhys.73.515

[14] L. Fornaro, C. Maidana, H. B. Pereira, A. Noguera, and A. Olivera, "Bismuth tri-iodide-Graphene 2D material," Journal of Crystal Growth, **639**, 127738 (2024). https://doi.org/10.1016/j.jcrysgro.2024.127738

[15] D. Cubicciotti, "Thermodynamic properties of bismuth (i) bromide and bismuth (iii) bromide," Inorganic Chemistry, **7**(2), 208-211 (1968). https://doi.org/10.1021/ic50060a005

[16] Z. Deng, F. Wei, Y. Wu, R. Seshadri, A. K. Cheetham, and P. Canepa, "Understanding the structural and electronic properties of bismuth trihalides and related compounds," Inorganic Chemistry, **59**(6), 3377-3386 (2020). https://doi.org/10.1021/acs.inorgchem.9b03214

[17] A. Darmawan, E. Suprayoga, A. A. AlShaikhi, and A. R. Nugraha, "Thermoelectric properties of two-dimensional materials with combination of linear and nonlinear band structures," Materials Today Communications, **33**, 104596 (2022). https://doi.org/10.1016/j.mtcomm.2022.104596

[18] N. R. Abdullah, B. J. Abdullah, H. G. Hussein, and V. Gudmundsson, "Novel ZnO nanosheet with buckling stress: First principles study of electronic, structural stability, phonon vibrations, lattice thermal and optical conductivity," Chemical Physics Letters, **844**, 141269 (2024). https://doi.org/10.1016/j.cplett.2024.141269

[19] D. Alfè, "Phon: A program to calculate phonons using the small displacement method," Computer Physics Communications, **180**(12), 2622-2633 (2009). https://doi.org/10.1016/j.cpc.2009.03.010

[20] A. Togo, and I. Tanaka, "First principles phonon calculations in materials science," Scripta Materialia, **108**, 1-5 (2015). https://doi.org/10.1016/j.scriptamat.2015.07.021

[21] J. P. Perdew, K. Burke, and M. Ernzerhof, "Generalized gradient approximation made simple," Physical review letters, **77**(18), 3865 (1996). https://doi.org/10.1103/physrevlett.77.3865

[22] K. Persson, Materials data on $BiBr_3$ (sg:14) by materials project, an optional note, (2016). https://doi.org/10.17188/1288706

[23] Y. Boran, and H. Kara, "A comprehensive density functional theory analysis on structural, electronic, and optical properties of BiOF," Brazilian Journal of Physics, **54**(5), 159 (2024). https://doi.org/10.1007/s13538-024-01523-w

[24] X. He, Y. Wu, S. Liu, W. He, S. Li, G. Huo, L. Jiang, *et al*., "Large-scale ultrastable 2D inorganic molecular crystal $BiBr_3$ and heterostructures with superior photoluminescence enhancement," Advanced Functional Materials, **34**(39), 2403273 (2024). https://doi.org/10.1002/adfm.202403273

[25] A. Jehan, M. Husain, S. Bibi, N. Rahman, V. Tirth, A. Azzouz-Rached, M. Y. Khan, *et al*., "Insight into the structural, optoelectronic, and elastic properties of AuXF3 (X= Ca, Sr) fluoroperovskites: Dft study," Optical and Quantum Electronics, **55**(14), 1242 (2023). https://doi.org/10.1007/s11082-023-05394-4

[26] A. Bafekry, M. Yagmurcukardes, B. Akgenc, M. Ghergherehchi, and B. Mortazavi, "First-principles investigation of electronic, mechanical and thermoelectric properties of graphene-like XBi (X= Si, Ge, Sn) monolayers," Physical Chemistry Chemical Physics, **23**(21), 12471-12478 (2021). https://doi.org/10.1039/d1cp01183a

[27] H. van Gog, W.-F. Li, C. Fang, R. S. Koster, M. Dijkstra, and M. van Huis, "Thermal stability and electronic and magnetic properties of atomically thin 2D transition metal oxides," npj 2D Materials and Applications, **3**(1), 18 (2019). https://doi.org/10.1038/s41699-019-0100-z

[28] N. R. Abdullah, B. J. Abdullah, and V. Gudmundsson, "DFT study of tunable electronic, magnetic, thermal, and optical properties of a Ga_2Si_6 monolayer," Solid State Sciences, **125**, 106835 (2022). https://doi.org/10.1016/j.solidstatesciences.2022.106835

[29] J. Xie, Z. Zhang, D. Yang, D. Xue, and M. Si, "Theoretical prediction of carrier mobility in few-layer BC_2N," The Journal of Physical Chemistry Letters, **5**(23), 4073-4077 (2014). https://doi.org/10.1021/jz502006z

[30] N. R. Abdullah, G. A. Mohammed, H. O. Rashid, and V. Gudmundsson, "Electronic, thermal, and optical properties of graphene like SiC_x structures: Significant effects of Si atom configurations," Physics Letters A, **384**(24), 126578 (2020). https://doi.org/10.1016/j.physleta.2020.126578

[31] Y. H. Shwan, M. A. Ameen, and A. S. Mahmood, "DFT study of electronic, optical, and thermodynamic properties of the 2D shape of Bi_4O_6 structure," Solid State Communications, **404**, 116095 (2025). https://doi.org/10.1016/j.ssc.2025.116095

[32] S. Qi, Y. Zhang, R. Zhang, X. Liu, and H. Xu, "First-principles and experiment investigation of Bi_2O_3/Bi_2WO_6 heterojunctions," Colloid and Interface Science Communications, **44**, 100502 (2021). https://doi.org/10.1016/j.colcom.2021.100502

[33] Y. H. Shwan, B. N. Ghafoor, and G. H. Hamasalih, "Optimization of surface plasmon resonance (SPR) for gold/air interface by using kretschmann configuration," Engineering and Technology Journal, **40**(10), 1334-1341 (2022). https://doi.org/10.30684/etj.2022.132902.1151

[34] H. Lashgari, A. Boochani, A. Shekaari, S. Solaymani, E. Sartipi, and R. T. Mendi, "Electronic and optical properties of 2D graphene-like ZnS: DFT calculations," Applied Surface Science, **369**, 76-81 (2016). https://doi.org/10.1016/j.apsusc.2016.02.042

[35] A. Akrap, J. Teyssier, A. Magrez, P. Bugnon, H. Berger, A. B. Kuzmenko, and D. Van Der Marel, "Optical properties of BiTeBr and BiTeCl," Physical Review B, **90**(3), 035201 (2014). https://doi.org/10.1103/physrevb.90.035201

[36] J.-L. Meyzonnette, J. Mangin, and M. Cathelinaud, ":Refractive index of optical materials," in: *Springer Handbook of Glass*, (Springer, 2019), pp. 997-1045. https://dx.doi.org/10.1007/978-3-319-93728-1_29

[37] A. Ghaleb, and A. Ahmed, "Structural, electronic, and optical properties of sphalerite ZnS compounds calculated using density functional theory (DFT)," Chalcogenide Letters, **19**(5), (2022). https://doi.org/10.15251/cl.2022.195.309

[38] I. T. Witting, T. C. Chasapis, F. Ricci, M. Peters, N. A. Heinz, G. Hautier, and G. J. Snyder, "The thermoelectric properties of bismuth telluride," Advanced Electronic Materials, **5**(6), 1800904 (2019). https://doi.org/10.1002/aelm.201800904

[39] M. Benaadad, A. Nafidi, S. Melkoud, M. S. Khan, and D. Soubane, "First-principles investigations of structural, optoelectronic and thermoelectric properties of Cu-based chalcogenides compounds," Journal of Materials Science, **56**(28), 15882-15897 (2021). https://doi.org/10.1007/s10853-021-06325-y

[40] X. Jiang, C. Ban, L. Li, C. Wang, W. Chen, and X. Liu, "Thermoelectric properties study on the BN nanoribbons via boltztrap first-principles," AIP Advances, **11**(5), 055120 (2021). https://doi.org/10.1063/5.0042555

[41] R. Chegel, "Enhanced electrical conductivity in graphene and boron nitride nanoribbons in large electric fields," Physica B: Condensed Matter, **531**, 206-212 (2018). https://doi.org/10.1016/j.physb.2017.12.053

[42] J. Androulakis, Y. Lee, I. Todorov, D.-Y. Chung, and M. Kanatzidis, "High-temperature thermoelectric properties of n-type pbse doped with Ga, In, and Pb," Physical Review B—Condensed Matter and Materials Physics, **83**(19), 195209 (2011). https://doi.org/10.1103/physrevb.83.195209

[43] J. Wang, L. P. Zhang, and Y. Li, "Preparation and analysis of novel thermoelectric material $(Sr_xCa_{1-x})_3Co_4O_9$," Applied Mechanics and Materials, **492**, 326-330 (2014). https://doi.org/10.4028/www.scientific.net/amm.492.326

[44] X. Tan, H. Shao, T. Hu, G. Liu, J. Jiang, and H. Jiang, "High thermoelectric performance in two-dimensional graphyne sheets predicted by first-principles calculations," Physical Chemistry Chemical Physics, **17**(35), 22872-22881 (2015). https://doi.org/10.1039/c5cp03466c

[45] Z.-X. Xie, L.-M. Tang, C.-N. Pan, Q. Chen, and K.-Q. Chen, "Ballistic thermoelectric properties in boron nitride nanoribbons," Journal of Applied Physics, **114**(14), 144311 (2013). https://doi.org/10.1063/1.4824750

[46] J. J. Plata, P. Nath, D. Usanmaz, J. Carrete, C. Toher, M. de Jong, M. Asta, *et al.*, "An efficient and accurate framework for calculating lattice thermal conductivity of solids: Aflow—aapl automatic anharmonic phonon library," npj Computational Materials, **3**(1), 45 (2017). https://doi.org/10.1038/s41524-017-0046-7

[47] Y.-Y. Wu, Q. Wei, J. Zou, and H. Yang, "Ultra-low thermal conductivity and high thermoelectric performance of monolayer BiP 3: a first principles study," Physical Chemistry Chemical Physics, **23**(35), 19834–19840 (2021). https://doi.org/10.1039/d1cp01383a

[48] M. Markov, Prediction of thermal conductivity and strategies for heat transport reduction in bismuth: an ab initio study., Ph.D. thesis, Universit'e Paris Saclay (COmUE) (2016).

[49] M. Wang, and D. Han, "Thermal properties of 2D dirac materials MN_4 (M= Be and Mg): a first-principles study," ACS omega, **7**(12), 10812-10819 (2022). https://doi.org/10.1021/acsomega.2c00785

[50] Y. Luo, X. Yang, T. Feng, J. Wang, and X. Ruan, "Vibrational hierarchy leads to dual-phonon transport in low thermal conductivity crystals," Nature communications, **11**(1), 2554 (2020). https://doi.org/10.1038/s41467-020-16371-w

[51] A. Togo, "First-principles phonon calculations with phonopy and phono3py," Journal of the Physical Society of Japan, **92**(1), 012001 (2023). https://doi.org/10.7566/jpsj.92.012001

ДОСЛІДЖЕННЯ СТАБІЛЬНОСТІ, ЕЛЕКТРОННИХ, ОПТИЧНИХ ТА ТЕПЛОВИХ ВЛАСТИВОСТЕЙ ДВОВИМІРНОГО НАПІВПРОВІДНИКА $BiBr_3$ ЗА ДОПОМОГОЮ DFT

Ядгар Хуссейн Шван, **Маджида Алі Амін**, **Арас Саїд Махмуд**

Фізичний факультет, Коледж освіти, Університет Сулеймані, Сулейманія 46001, Курдистан, Ірак

Теорія функціоналу густини (DFT) служить методом перших принципів для ретельного дослідження стабільності структури та аналізу електронних, оптичних та теплових характеристик двовимірного трибромiду вісмуту (2D $BiBr_3$). Моделювання молекулярної динаміки ab-initio (AIMD) показує, що структура є термічно стабільною при 300 K. $BiBr_3$ поводиться як напівпровідник із забороненою зоною 2,84 еВ згідно з його електронною зонною структурою та аналізом часткової густини станів (PDOS). Оптична характеристика показує, що $BiBr_3$ має сильні взаємодії у видимому та ультрафіолетовому діапазонах довжин хвиль, що демонструє його потенціал у наступному поколінні оптичних та оптоелектронних пристроїв. Чудове значення термоЕРС, оцінене за допомогою розрахунків переносу Больцмана, підкреслює перспективність $BiBr_3$ у низькотемпературному термоелектричному управлінні. Це дослідження передбачає покращення коефіцієнта потужності, зумовленого температурою, яке досягає піку в 3,25 $\times 10^{12}$ Вт/K^2·см·с при 300K. $BiBr_3$ демонструє помірну теплоємність при середніх та високих температурах, зберігаючи при цьому дуже низьку теплопровідність. Це підкреслює його здатність ефективно керувати теплом та служити ізолятором у різних застосуваннях. Детальні результати показують, що 2D $BiBr_3$ є потенційно сприятливим матеріалом з різноманітними можливостями в більшості технологічних застосувань.

Ключові слова: *структура $BiBr_3$; DFT; стабільність; електронні характеристики; теплові властивості; оптичні характеристики*